Bull Volcanol (2014) 76:784
DOI 10.1007/s00445-013-0784-4

RESEARCH ARTICLE

A global database of composite volcano morphometry

Pablo Grosse · Pablo A. Euillades · Leonardo D. Euillades · Benjamin van Wyk de Vries

Received: 28 June 2013 / Accepted: 6 November 2013

Abstract We present a global database on the subaerial morphometry of composite volcanoes. Data was extracted from the 90-m resolution Shuttle Radar Topography Mission (SRTM) digital elevation model (DEM). The 759 volcanoes included in the database are the composite (i.e., polygenetic) volcanoes listed in the Smithsonian Institution Global Volcanism Program (GVP) database that are covered by the SRTM DEM, have a constructional topography and a basal width larger than 2 km. The extent of each volcano edifice was defined using the NETVOLC algorithm, which computes outlines by minimizing a cost function based on breaks in slope around the edifices. Morphometric parameters were then calculated using the MORVOLC algorithm. The parameters characterize and quantify volcano size (basal width, summit width, height, and volume), profile shape (height/basal width and summit width/basal width ratios), plan shape (ellipticity and irregularity indexes), and slopes. In addition, 104 well-defined and relatively large summit craters/calderas were manually delineated and specific parameters were computed. Most parameters show large variation without clear separations, indicating a continuum of volcano morphologies. Large overlap between the main GVP morphologic types highlights the need for a more rigorous quantitative classification of volcano morphology. The database will be maintained and updated through a website under construction.

Keywords Composite volcano · Morphometry · Database · SRTM DEM

Editorial responsibility: A. Gudmundsson

Electronic supplementary material The online version of this article (doi:10.1007/s00445-013-0784-4) contains supplementary material, which is available to authorized users.

P. Grosse (✉)
CONICET and Fundación Miguel Lillo, Miguel Lillo 251, 4000 San Miguel de Tucumán, Argentina
e-mail: pablogrosse@yahoo.com

P. A. Euillades · L. D. Euillades
Instituto CEDIAC, Universidad Nacional de Cuyo, Ciudad Universitaria, 5500 Mendoza, Argentina

B. van Wyk de Vries
Laboratoire Magmas et Volcans, UMR6524-CNRS, IRD, OPGC, Université Blaise Pascal, 5 Rue Kessler, 63038 Clermont-Ferrand, France

Introduction

Volcano morphologies result from the interaction through time of constructive and destructive geological and environmental processes. Given the large number and complexity of these processes, volcanoes occur in a wide variety of shapes and sizes. They are generally constructional landforms with positive topographies, but can also be excavational (calderas, maars) or lack a clear topographic expression (e.g., fissure vents and ignimbrite sheets). Their shapes can vary from the ideal symmetrical cone to very irregular volcanic chains or massifs. Their sizes can vary from small monogenetic cones of a few tens of meters in height and a few hundreds of meters in diameter to huge massifs of several thousand meters in height and several tens of kilometers in diameter. Quantitative volcano morphology (i.e., volcano morphometry) is of interest because it can supply information concerning the processes that interact during the growth history and evolution of volcanoes. Although shape and size are basic volcano properties, there is to date no comprehensive database of volcano morphometry at a global scale.

We here present a systematic near-global database on the morphometry of composite volcanoes. We use the term 'composite volcano' as defined by Davidson and De Silva (2000), i.e., all constructional and polygenetic volcanoes, including both 'composite cones' (synonymous to stratovolcano) and 'shield volcanoes'. The database consists of morphometric

Published online: 13 December 2013

parameters that thoroughly characterize the shape and size of volcano edifices in a systematic and comparable way. The morphometric data was extracted from the Shuttle Radar Topography Mission (SRTM) digital elevation model (DEM). Considered volcanoes are the composite constructional volcanoes listed in the Smithsonian Institution Global Volcanism Program database (Siebert et al. 2010) covered by the SRTM DEM. Thus, the database includes most of the subaerial active or potentially active composite volcanoes of the world. The goal of this contribution is to present the database, describing the applied methodology and the database design. We also perform a general analysis of the data, although more detailed analyses are beyond the scope of this contribution. We anticipate that the database will become a useful tool for research on a variety of volcanological processes and at several scales.

Compilations and studies on composite volcanoes containing morphometric data

There are many studies on monogenetic cone fields containing morphometric measurements (e.g., Favalli et al. 2009; Kervyn et al. 2012, and references therein), but relatively few on composite volcanoes. The most complete existing database at a global scale containing volcano morphometric parameters is that of Pike (1978) and its revision, Pike and Clow (1981). This compilation contains 697 entries, including composite volcanoes, calderas, and monogenetic cones. It considers five measurements, three of which relate to the summit crater (edifice height and flank width; crater diameter, depth, and circularity).

Several regional compilations or catalogues contain varied volcano morphometric data. Compilations include those of Japan (Committee for Catalog of Quaternary Volcanoes in Japan 1999), Kamchatka (Fedotov and Masurenkov 1991; Kozhemyaka 1995), Alaska (Miller et al. 1998), North America (Wood and Kienle 1990), Central America (van Wyk de Vries et al. 2007), and the Central Andes (De Silva and Francis 1991). The morphometric data in these contributions is limited, generally not more than height and/or basal diameter are given, although in some cases volume estimations or crater dimensions are also provided. The variability in data sources and in the methods used for estimating parameters greatly limits cross-comparisons between these compilations.

More detailed studies focusing on a specific region, volcano type, and/or measurement also contain morphometric data, such as slope analysis of shield volcanoes (Mouginis-Mark et al. 1996; Rowland and Garbeil 2000), volume estimations of stratovolcanoes within an arc segment (Stoiber and Carr 1973; Carr 1984; Carr et al. 2007; Völker et al. 2011), shape characterization of symmetrical cones (Karátson et al. 2010), or calculation of stratovolcano erosion rates (Karátson et al. 2012). Again, data quality and methods vary and comparisons are difficult. Detailed studies on individual or a few volcanoes often give some morphometric data such as height, volume, slopes, etc. (e.g., Favalli et al. 2005; Mathieu et al. 2013), but again data are drawn from diverse sources, reducing their value for entry into a global database. Of special notice is the morphometric characterization of Martian shields by Plescia (2004) because, by using a planet-wide dataset, the Mars Orbiter Laser Altimeter (MOLA) DEM, it has the advantage, as we seek here, to be truly comparable. There is also considerable morphometric data on seamounts derived from bathymetric DEMs (e.g., Stretch et al. 2006; Mitchell et al. 2012). However, as yet there is no bathymetric dataset equivalent to the SRTM DEM.

Methodology

DEM source and volcano selection

We have used the C-band 3 arc seconds (~90 m spatial resolution) SRTM DEM (e.g., Rabus et al. 2003) to compile the database. It is at present the most adequate DEM dataset because it has a near-global coverage, a spatial resolution that is sufficient for morphometric analysis of composite volcanoes (e.g., Wright et al. 2006; Kervyn et al. 2008; Grosse et al. 2009) and good accuracy (e.g., Rodríguez et al. 2006). We used the seamless SRTM DEM dataset from CGIAR-CSI (Consultative Group on International Agricultural Research–Consortium for Spatial Information; Jarvis et al. 2008). Although the ASTER Global Digital Elevation Model (G-DEM) has a better spatial resolution of 30 m, it suffers from numerous errors and artifacts that strongly limit its use in morphometric studies (e.g., Reuter et al. 2009; Grosse et al. 2012).

Selection of the volcanoes for the database was based on the Smithsonian Institution's Global Volcanism Program (GVP) compilation of active and potentially active volcanoes of the world (Siebert et al. 2010). The GVP catalogue lists 1,545 volcanoes worldwide (Fig. 1). Of these, entries with one or more of the following features were discarded from our database: (1) volcanoes not covered by the SRTM DEM dataset above latitudes 60° N and 56° S ($n=80$); (2) submarine and subglacial volcanoes ($n=145$); (3) monogenetic cones, domes, and shields ($n=345$); (4) volcanoes with no discernible positive topographies or with mostly negative topographies (i.e., calderas, maars, and lava fields; $n=148$); (5) volcanoes with no discernible topographic boundaries ($n=47$); and (6) volcanoes with basal widths <2 km (arbitrary limit established to discard edifices that are too small to accurately analyze with the 90-m SRTM DEM resolution; $n=53$). The remaining volcanoes are included in our database. They are classified in the GVP database as stratovolcano(es),

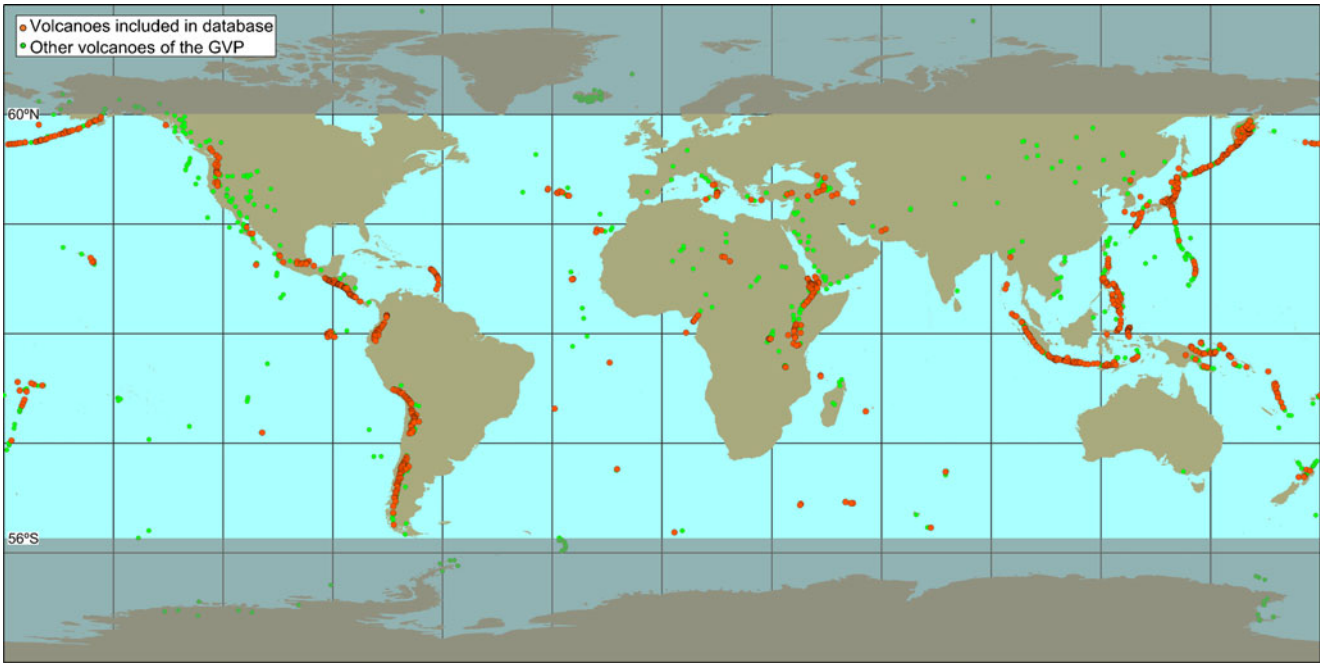

Fig. 1 World map showing location of volcanoes included in our database and of all other volcanoes of the Smithsonian Institution Global Volcanism Program (*GVP*) database

complex volcano, compound volcano, somma volcano(es), shield volcano(es), pyroclastic shield, lava cone, lava dome(s), or unknown. Some volcanoes listed as 'stratovolcanoes' or 'complex volcano' contain clearly separate edifices; in these cases we obtained data for the main edifice(s) and sometimes also for the whole massif. Conversely, in a few cases two edifices forming a twin massif are listed separately as 'stratovolcano'; in these cases we have considered each edifice as well as the whole massif. We have also included seven post-caldera edifices that are listed as 'caldera' in the GVP database. In total, our database has 759 entries (Fig. 1).

Volcano edifice boundary delineation

The first step towards obtaining morphometric data is to define the extent or basal outline of each volcano. This is a key issue because the resulting morphometric parameter values can vary considerably depending on the estimated outline, especially true for size parameters, such as height, width, and volume (Grosse et al. 2012). Defining volcano boundaries is a complicated task due to the great variety and complexity of volcanic terrains (e.g., merging with surrounding landscape, erosional and collapse features, and far-reaching lava flows). Nevertheless, constructional volcanoes are generally characterized by edifices with positive topography that are bounded by concave breaks in slope. This difference in slope gradient between edifice and surrounding terrain has been the basis for boundary delineation in most volcano morphometric studies, both of monogenetic scoria cones (e.g., Favalli et al. 2009; Kervyn et al. 2012, and references therein) and of composite volcanoes (e.g., Pike 1978; Plescia 2004; Grosse et al. 2009, 2012; Völker et al. 2011; Karátson et al. 2012).

The usual approach for delimitation of volcano edifices is the manual tracing of slope-breaks using one or a combination of DEM-derived products (Smith and Clark 2005; Evans 2012). Although manual delineation can benefit from user experience and expertise, it is inevitably dependent on user subjectivity. In order to minimize subjectivity, and thus maximize consistency and hence comparability, we have applied an expressly developed algorithm, NETVOLC (Euillades et al. 2013). Given a DEM and the approximate center of the volcano, NETVOLC computes an outline by minimizing a cost function defined from several DEM-derived products. In a first stage, a main cost function is applied that considers only convexity and aspect, and in a second stage three alternative functions can be applied (useful in complex cases) which also consider slope, elevation, and/or radial distance; for details see Euillades et al. (2013). In practice, for each volcano of the database we cut a portion of the SRTM DEM containing the edifice and selected a central pixel. With this input NETVOLC calculated edifice outlines for each volcano using the main cost function. Unsatisfactory results (e.g., outlines along slope-breaks within edifices at high gradients and outlines following slope-breaks on neighboring landforms), identified visually, were re-processed applying an alternative cost function selected by the user; particularly problematic cases were very flat shields, edifices that are part of a mountainous chain with complicated topography, and cones with very smooth concave-up profiles that merge almost completely with the surroundings. This introduces some degree of

subjectivity and semi-automation. Still, the method is more objective, and faster, than the manual alternative.

Other approaches to volcano delimitation are possible, using additional data such as optical satellite images, geological maps, and/or field knowledge. However, the use of different data sources will affect the consistency and comparability of the resulting outlines. By considering only topography and using only one global DEM as data source, we ensure the best possible consistency of the results.

It should be noted that our approach delimits volcano edifices only; flat-lying ring plains and other far-reaching volcanic products are excluded. Thus, size parameters will consider the edifice and not all of the volcanic products; resulting values will be smaller than those obtained if considering all of the products. Also to keep in mind is that for volcanic islands where the edifice continues underwater, only the subaerial part of the edifice is considered, since the SRTM DEM does not contain bathymetric data. This is the case for 218 edifices in our database; of these, 102 partially continue underwater and 116 totally continue underwater. The size parameters for these edifices will be underestimations.

In addition to the basal outlines, well-defined summit craters or calderas of 104 edifices were manually delineated (we do not attempt to distinguish between 'crater' and 'caldera', hereon we use the term 'crater' indistinctly). This was done in order to mask out the crater when calculating edifice flank slopes, but also enabled the computation of crater-specific morphometric parameters. Manual delineation was quite straightforward, since only craters with clear topographic breaks were considered. Given the SRTM DEM spatial resolution, we were only able to delineate relatively large craters (average width >0.6 km); thus, the crater data in our database should not be taken as a comprehensive crater dataset.

Morphometric parameter computation

Given the edifice outlines and the SRTM DEM, morphometric parameters for each volcano edifice were computed using another expressly developed algorithm, MORVOLC (Grosse et al. 2009, 2012). The set of parameters thoroughly and quantitatively describe the morphology of each edifice. Below are brief descriptions of the parameters computed by MORVOLC and Fig. 2 illustrates the main parameters; for details of the parameters and evaluation in terms of boundary delineation and DEM source see Grosse et al. (2012).

The edifice outline is used to directly compute basal area, average basal width (measured as the diameter of an area-equivalent circle), and major and minor basal axes. For the calculation of edifice height and volume, a 3D basal surface is fitted to the basal outline. Although we previously used Triangular Irregular Network (TIN) surfaces (Grosse et al. 2012), from subsequent testing of different interpolation methods we find inverse distance weighting (IDW) to be more

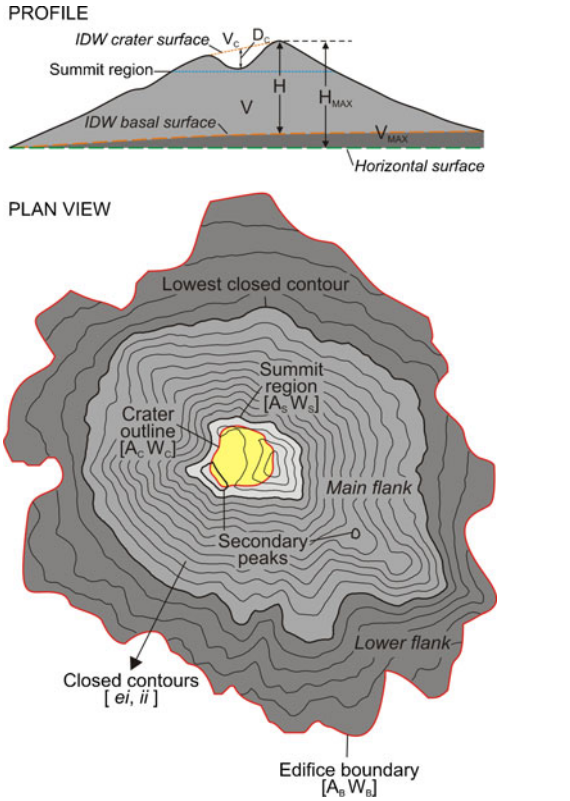

Fig. 2 Schematic cross-section and plan view of a volcano edifice showing main morphometric parameters: height (H), maximum height (H_{MAX}), volume (V), maximum volume (V_{MAX}), crater depth and volume (D_C, V_C), basal area and width (A_B, W_B), summit region area and width (A_S, W_S), crater area and width (A_C, W_C), closed contour ellipticity and irregularity indexes (ei, ii), and secondary peaks

accurate; this interpolation method was used for computations of height and volume. Maximum heights and volumes are also computed considering a horizontal base with elevation equal to the lowest edifice outline point. The difference between IDW-derived and maximum values will depend on the dip and irregularity of the terrain onto which the edifice stands. When edifices coalesce, the IDW-derived values will be underestimations; the 'real' heights and volumes will be between the IDW-derived and the maximum values.

Elevation contours are generated at 50-m intervals. One contour is selected as the limit between edifice flank and summit region. For edifices with summits bounded by only one main contour per elevation value, this limit is the elevation at which the rate of slope decrease is greatest (where convexity is maximum). For more complex summits bounded by more than one main contour per elevation value, the limit will be the elevation of the uppermost unique contour before the division into two or more main contours occurs. From this contour, summit area and width are calculated. Furthermore, the flank is separated into lower flank and main flank at the elevation of the lowest closed elevation contour.

Edifice profile shape is summarized using two dimensionless size ratios, height/basal width and summit width/basal

width. The first ratio estimates overall steepness, and the second ratio estimates the degree of pointedness or truncation of the edifice.

For each closed elevation contour bounding the edifice flank, two independent dimensionless indexes are computed, ellipticity (quantifies the elongation of each contour) and irregularity (quantifies the irregularity or complexity of each contour). These indexes summarize the plan shape of the edifice at successive heights, and the average values give an overall estimation.

A DEM-derived slope map is used to compute several average slope values: of the whole edifice, of the flank (including total flank, lower flank, and main flank), of the summit region, and of each successive 50-m height interval. Furthermore, the value of the interval with highest average slope is defined as the maximum average slope for the edifice.

Azimuths of the major basal axis and the average azimuth of the major axes of each closed elevation contour bounding the edifice flank are computed. These values indicate the geographic orientation of edifice elongation.

Secondary elevation contours (i.e., small closed contours produced by peaks or craters) are counted as secondary peaks or holes. These values give an estimation of terrain roughness, and also relate to the number of secondary vents, but are very dependent on DEM source and resolution (Grosse et al. 2012).

If a summit crater was delineated, MORVOLC computes several additional crater-related parameters: area, average width, major axis, azimuth of the major axis, depth and volume (by fitting a 3D IDW surface to the crater outline), ellipticity and irregularity of the crater outline, and average slope. The crater is either contained within the summit region or, if there is no significant slope decrease or no closed contour below the crater outline, it is directly used as the limit of the summit region (and thus summit and crater sizes are equal). If a crater is considered, edifice slope values exclude the slopes within the crater in their computations. Thus, if the crater outline is considered as the summit region there will be no summit region average slope and the total and flank slopes will be equal. Furthermore, secondary peaks and holes are not counted within craters.

Database design

The database is presented as an Excel spreadsheet (Online Resource 1). Data are in columns and each volcano entry occupies a row. The database consists of a main worksheet 'Parameters' and four additional worksheets containing arrays of data.

The main worksheet is ordered as follows:

- Columns A to D contain data taken from the GVP database: volcano number, name, geographical location, and type. For entries that differ from the GVP compilation as explained in Section "DEM source and volcano selection", we have added the appropriate name and/or type between brackets, and the situation is stated in column E.
- Column E lists problems or particularities that stood out during delineation of edifice outline and/or acquisition of morphometric parameters.
- Column F indicates if a summit crater is considered, and column G contains observations about the crater, in particular if the crater outline is used as the summit region; it also indicates identified craters that were not delineated, either because they are incomplete, unclear, or not on the summit (37 cases), or because they are too small (98 cases).
- Column H indicates if the edifice continues underwater, either totally or partially.
- Columns I and J give the latitude and longitude of the highest elevation pixel, as obtained from the SRTM DEM.
- Columns K and L give the minimum and maximum elevations of the edifice; note that the maximum elevation is that of the SRTM DEM and thus is different than that given in the GVP database (it is generally lower because the SRTM DEM smoothes out the relief and no point elevations are considered).
- Columns M to V contain size parameters (in metric units): basal area, average basal width, minor basal axis, major basal axis, summit region area, average summit region width, height, maximum height, volume, and maximum volume.
- Columns W and X contain the two profile shape parameters (dimensionless): height/basal width ratio and summit width/basal width ratio.
- Columns Y to AB contain the plan shape parameters (dimensionless): ellipticity and irregularity indexes of the basal outline and average ellipticity and irregularity indexes of the main flank elevation contours.
- Columns AC to AI contain slope values (in degrees): mean slope of the whole edifice, flank, lower flank, main flank, and summit region; maximum average slope and its height fraction.
- Columns AJ and AK contain orientation parameters (in degrees): azimuth of major basal axis and average azimuth of elevation contour major axes bounding the edifice flanks.
- Columns AL to AQ contain the number of secondary peaks and holes: peak count of the whole edifice, of the flank and of the summit region, and hole count of the whole edifice, of the flank, and of the summit region.
- Columns AR to AX contain additional data on the elevation contours: number of main closed elevation contours on flank and summit region; elevation, elevation fraction (with regard to the maximum edifice height), and average

width of lowest closed contour; and elevation and elevation fraction of contour defined as start of summit region.
- Columns AY to BO contain summit crater parameters: minimum crater elevation in meters and as fraction of the edifice elevation, crater area, average crater width, major crater axis, azimuth of the major crater axis, crater depth, maximum crater depth, crater volume, maximum crater volume, crater outline ellipticity and irregularity, crater depth/crater width ratio, crater width/edifice basal width ratio, crater depth/edifice height ratio, crater volume/edifice volume ratio, and mean slope within the crater.

The four additional worksheets contain arrays of ellipticity and irregularity values of elevation contours, average slopes of height intervals, and slope frequencies. In all of these worksheets, columns A to C are the same as for the main worksheet, containing number, name, and location. The worksheets are ordered as follows:

- 'Ellipticity index': column D indicates the number of main closed elevation contours on the flank, columns E and F give the elevations of the lowest closed contour and of the start of the summit region, and column G onward contains the ellipticity index of each flank contour.
- 'Irregularity index': columns D to F are the same as the previous worksheet, and column G onward contains the irregularity index of each flank contour.
- 'Slopes': columns D to G indicate the number of slope bins, the elevation of the lowest bin (value given is the upper limit, i.e., '50' means the bin considers elevations between 0 and 50 m), elevation of the lowest closed contour and the elevation of the start of the summit region; column H onward contains the mean average slope of each bin at successive 50-m height intervals.
- 'Slope histograms': columns D to AU contain the percent frequency of slopes at 1° intervals from 0–1° to 43–44°, for the whole edifice.

Database analysis

We here make a general analysis of the database; more detailed analyses, including classification schemes or regional comparisons, are not the objective of this paper. Table 1 lists statistics of the main morphometric parameters for all entries, grouped by their underwater extent (whether they continue underwater or not), and grouped into four morphological types, obtained by simplifying the GVP classification: (1) stratovolcano, (2) stratovolcanoes, (3) complex/compound/somma volcano, and (4) [pyroclastic] shield(s) volcano(es). Parameter histograms and statistics considering all entries are shown in Fig. 3; Fig. 4 consists of X–Y plots showing correlations between parameters, in which the data are discriminated by type and underwater extent; and Fig. 5 shows box-plots of parameters for all entries and grouped according to the four main morphological types.

Main parameters

Because most parameters do not show normal distributions (Fig. 3), in the following analysis we consider median instead of mean averages, and ranges excluding outliers that are 3× IQR (inter-quartile range) above the third quartile or below the first quartile.

Size

Size parameters vary greatly and have strong to weak positive asymmetric distributions (Fig. 3a–d). Ranges are 2–34 km basal widths, 0.1–3.10 km heights, and 0.2–160 km^3 volumes. Basal width and especially volume values contain many outliers, with maximum values of 66 and 3,000 km^3, respectively. Note that minimum values reflect the cutoff dictated by the SRTM DEM resolution; the smallest composite volcanoes (not included in the database) have basal widths of ~1 km. Medians considering all entries are 8.8 km basal width, 1.02 km height, and 16 km^3 volume. Edifices that continue underwater have on average smaller subaerial sizes (Table 1), reflecting the underestimation of these parameters; discarding this group, the medians are 9.3 km basal width, 1.10 km height, and 20 km^3 volume. Summit region width for all entries ranges from 0.2 to 10 km, with a median of 1.5 km.

Height correlates positively with both basal width and volume (Fig. 4a–b). The data plotted in these graphs show clear-cut upper limits, suggesting for a critical maximum steepness threshold, whereas the lower limits are diffuse. In the height vs. basal width graph (Fig. 4a), the upper limit is greater than the linear ratio of height=0.2×basal width proposed by Settle (1979) as a maximum ratio for fresh scoria cones. It is best fitted by a power-law trend (Fig. 4a), suggesting that maximum steepness is not constant but decreases with increasing size. Summit and basal widths show a weak positive correlation (Fig. 4c).

Profile shape: height/width ratios

The height/basal width ratio (H/W_B) shows quite a flat and symmetric distribution (Fig. 3e), with mean and median averages of 0.12. Values range from 0.01 to 0.30. The distribution of the summit width/basal width ratio (W_S/W_B) is more positively skewed and has a larger spread (Fig. 3f). Values range from 0.02 to 0.76; the median is 0.19. These ratios are not significantly different between edifices that continue underwater from those that do not. The average H/W_B ratio is comparable to averages obtained for scoria cones of mostly

Table 1 Statistics of the main morphometric parameters for all entries of the database and grouped according to their underwater extent (whether they continue underwater or not) and to four main morphological types following the Smithsonian Institution Global Volcanism Program (GVP) database

	Basal width (km)	Height (km)	Volume (km^3)	Summit region width (km)	Height/ basal width	Summit width/ basal width	Ellipticity index (avg.)	Irregularity index (avg.)	Mean slope (total)	Mean slope (flank)	Mean slope (lower flank)	Mean slope (main flank)	Mean slope (summit)	Max avg slope	Max avg slope (height fraction)	Sec peaks (total)	Holes (total)	*Assigned craters*
All entries *(n=759)*																		*104 (14 %)*
Median	8.8	1.02	16	1.5	0.12	0.19	1.72	1.18	16.7	16.6	14.5	20.2	18.3	25.1	0.77	5	0	
Mean	10.7	1.11	57	2.4	0.12	0.22	1.83	1.30	16.5	16.3	14.4	19.9	18.2	24.4	0.73	11	1	
Standard deviation	7.5	0.56	185	2.4	0.05	0.15	0.57	0.37	5.1	5.2	5.1	6.1	5.5	8.0	0.17	20	3	
Minimum	2.0	0.10	0.2	0.2	0.01	0.02	1.09	1.01	1.8	1.7	1.7	3.6	3.4	2.0	0.11	0	0	
Maximum	65.9	4.57	3,086	16.3	0.30	0.76	5.23	3.73	33.3	32.5	37.0	36.9	35.8	42.8	0.97	230	24	
Underwater extent																		
Do not continue underwater (*n*=541)																		*70 (13 %)*
Median	9.3	1.10	20	1.4	0.12	0.18	1.70	1.18	16.9	16.7	14.5	20.8	18.4	26.4	0.79	5	0	
Mean	11.0	1.18	55	2.2	0.12	0.20	1.79	1.30	16.6	16.4	14.6	20.3	18.6	25.1	0.77	11	1	
Standard deviation	6.9	0.56	158	2.3	0.05	0.13	0.53	0.36	4.7	4.8	4.6	5.8	5.3	7.9	0.13	21	3	
Minimum	2.0	0.10	0.2	0.2	0.01	0.02	1.09	1.01	1.8	1.7	1.7	4.4	4.4	2.1	0.18	0	0	
Maximum	65.9	4.57	3,008	16.3	0.26	0.70	4.35	3.73	28.3	28.3	27.2	36.9	33.6	42.8	0.97	230	24	
Continue underwater (*n*=218)																		*34 (16 %)*
Median	7.4	0.82	10	1.7	0.11	0.23	1.76	1.18	16.3	16.2	13.7	19.1	17.5	23.0	0.66	4	0	
Mean	10.0	0.93	61	2.7	0.12	0.28	1.92	1.30	16.2	16.1	13.9	19.0	17.1	22.8	0.63	10	1	
Standard deviation	8.7	0.52	238	2.7	0.06	0.17	0.67	0.37	6.1	6.2	6.1	6.7	5.7	8.2	0.21	17	2	
Minimum	2.0	0.14	0.3	0.2	0.02	0.02	1.11	1.01	2.6	2.0	2.0	3.6	3.4	2.0	0.11	0	0	
Maximum	63.3	3.03	3,086	12.6	0.30	0.76	5.23	3.01	33.3	32.5	37.0	35.3	35.8	40.2	0.95	167	14	
Volcano type																		
Stratovolcano (*n*=512)																		*65 (13 %)*
Median	7.9	1.02	14	1.1	0.13	0.16	1.63	1.15	17.7	17.7	15.0	21.5	19.1	27.7	0.79	3	0	
Mean	9.4	1.13	42	1.8	0.14	0.20	1.73	1.26	17.8	17.7	15.4	21.5	19.1	26.8	0.75	8	1	
Standard deviation	6.2	0.55	151	2.0	0.05	0.14	0.51	0.34	4.5	4.6	4.7	5.3	4.9	6.8	0.16	18	2	
Minimum	2.0	0.17	0.3	0.2	0.02	0.02	1.09	1.01	6.4	5.7	3.0	7.7	5.1	9.0	0.11	0	0	
Maximum	65.9	4.57	3,008	16.3	0.30	0.74	4.35	3.73	33.3	32.5	37.0	36.9	35.8	42.8	0.97	230	22	
Stratovolcanoes (*n*=87)																		*6 (7 %)*
Median	10.5	1.06	27	2.4	0.11	0.28	1.95	1.25	16.3	16.1	14.4	18.9	18.0	22.4	0.73	7	0	
Mean	10.8	1.16	43	2.9	0.11	0.28	2.04	1.33	16.7	16.3	14.8	19.7	19.0	23.4	0.70	11	1	
Standard deviation	4.9	0.50	49	2.1	0.04	0.17	0.60	0.31	3.4	3.7	4.0	4.4	4.5	6.3	0.19	11	2	
Minimum	2.3	0.29	0.3	0.3	0.05	0.03	1.22	1.03	11.0	9.3	6.6	9.2	9.5	11.0	0.21	0	0	
Maximum	25.0	2.42	273	10.0	0.22	0.76	4.15	2.96	26.0	26.2	25.7	29.0	29.5	36.9	0.96	69	11	
Complex/compound (*n*=66)																		*4 (6 %)*
Median	10.4	1.14	27	2.4	0.09	0.28	2.11	1.40	16.5	16.3	14.5	18.4	19.2	21.3	0.72	8	1	
Mean	12.7	1.13	66	3.5	0.10	0.27	2.18	1.56	16.1	15.7	14.2	18.8	18.8	22.1	0.71	19	3	
Standard deviation	7.3	0.48	117	2.8	0.04	0.14	0.49	0.52	3.7	3.7	3.9	4.8	5.2	6.4	0.15	27	4	
Minimum	3.5	0.19	1.3	0.3	0.04	0.03	1.22	1.06	7.6	7.7	5.1	7.6	4.4	8.2	0.12	0	0	
Maximum	38.4	2.67	779	11.9	0.19	0.60	3.26	3.18	24.6	24.6	24.2	30.6	28.3	36.0	0.95	146	24	
Shield(s) (*n*=89)																		*29 (33 %)*
Median	15.3	0.81	31	3.5	0.06	0.28	1.98	1.24	8.1	8.1	6.7	9.7	10.6	11.8	0.67	9	1	
Mean	17.1	0.94	150	4.2	0.06	0.29	2.11	1.34	9.0	8.9	8.0	10.5	11.0	12.7	0.64	19	2	
Standard deviation	11.6	0.67	371	3.0	0.03	0.16	0.81	0.42	4.4	4.5	4.8	4.9	5.1	6.5	0.20	27	3	
Minimum	2.3	0.10	0.2	0.4	0.01	0.02	1.13	1.02	1.8	1.7	1.7	3.6	3.4	2.0	0.18	0	0	
Maximum	63.3	3.03	3,086	12.3	0.18	0.64	5.23	3.14	22.5	22.8	22.7	24.8	26.2	31.9	0.96	167	14	

0.10 to 0.16, whereas the average W_S/W_B ratio is lower than the average crater width/basal width ratios for scoria cones of mostly 0.25 to 0.50 (Favalli et al. 2009; Kervyn et al. 2012; Fornaciai et al. 2012).

H/W_B tends to decrease with size (Fig. 4d); edifices with basal widths >20 km have $H/W_B \leq 0.11$, and all edifices with $H/W_B > 0.17$ have basal widths <14 km. Conversely, the W_S/W_B ratio varies considerably but is not correlated significantly with size (Fig. 4e). Although showing large scatter, the H/W_B and W_S/W_B ratios are negatively correlated (Fig. 4f); edifices with high H/W_B ratios have relatively small summits, whereas edifices with low H/W_B ratios can have small or large summits. An analogy can be made with scoria cones, where the formation of a large crater truncates the cone, decreasing its height (Kervyn et al. 2012).

Plan shape: ellipticity and irregularity indexes

The average ellipticity (*ei*) and irregularity (*ii*) values (only considering edifices with five or more closed elevation contours, 597 entries) have positive asymmetric distributions; the *ii* distribution is more strongly skewed, whereas the *ei* distribution has greater spread (Fig. 3g–h). Average *ei* values range from 1.1 to 4.1 (median=1.72). Average *ii* values range from 1.0 to 2.3 (median=1.18). There is no significant difference in these values between edifices that continue underwater from those that do not.

There is a weak positive correlation between the two indexes (Fig. 4g). Two rough trends can be considered, one of greater *ei* in relation to *ii* (elongated edifices that are not so irregular) and the other of greater *ii* in relation to *ei* (irregular edifices that are not so elongated). The indexes lack significant correlation with size (Fig. 4h–i), although larger edifices tend to have higher values. Both indexes show rough negative correlations with the H/W_B ratio (Fig. 4j–k), suggesting that lower H/W_B ratios can be related to increasing complexity (e.g., vent migration and erosion/dissection).

Slopes

Slope parameter distributions are symmetric to slightly negatively skewed (Fig. 3i–k). Average slopes, considering either the whole edifice or only the flank, range from 2 to 33° with a median of 17°. The medians for the lower flanks and main flanks are 15° and 20°, respectively. Maximum average slopes range from 2 to 43° (median=25°). The height fraction where maximum slopes occur ranges from 0.1 to 1 (median=0.77). Slope statistics are similar between edifices that continue underwater and those that do not.

Average slopes (both total and flank) tend to decrease with size (Fig. 4l) and correlate positively with the H/W_B ratio (Fig. 4m). For a given H/W_B ratio, flank slope increase can be related to greater truncation (e.g., Kervyn et al. 2012), dissection and/or local irregularities such as secondary vents.

Secondary peaks

Secondary peak count has a strong positive distribution (Fig. 3l) with values ranging from 0 to 40 (with several outliers to a maximum of 230) and a median of 5. Peak count correlates positively with size and with average *ii* (Fig. 4n–o). It can be considered an estimation of complexity; all edifices with average *ii* >1.8 have nine or more secondary peaks, but edifices with low average *ii* can also have many secondary peaks.

Crater parameters

Only relatively large craters were delineated and thus the crater data in our database is incomplete; statistics provided below should not be considered representative of the entire population of summit craters. Crater widths range between 0.6 to 11 km; the median is 2.2 km. Crater depths range from under 100 to 860 m; the median is 240 m. Crater volumes range from less than 0.1 to over 10 km^3, with a median of 0.5 km^3. The crater depth/crater width ratio (D_C/W_C) is very variable, from 0.01 to 0.29, with a median of 0.11. The ratio tends to decrease with increasing crater size (width and volume). Crater widths correlate with edifice basal and summit region widths, but there is no correlation between crater depth and edifice height. The D_C/W_C ratio roughly correlates with the H/W_B ratio, i.e., inner crater steepness correlates positively with outer edifice steepness. Considered craters are found in flatter than average edifices (median H/W_B ratio of edifices with an assigned crater is 0.08).

Morphological types

Comparison of parameters between the four main GVP morphologic types indicates poor separation between types, with most parameters having large spread and almost complete overlap (Figs. 4–5). The clearest difference is that, as expected, shields are flatter, and thus have lower H/W_B ratios and slopes (Figs. 4–5). However, several edifices classified as shields have H/W_B and slope values that are much higher than expected for a shield volcano (e.g., Tolbachik and Tristan da Cunha). Also, large summit craters are more common on shields: 33 % of shields (29 of 89) have an assigned crater, whereas only 11 % of the other three types have them.

A rough transition can be considered from ‘stratovolcano’ to ‘stratovolcanoes’ to ‘complex/compound volcano’ of increasing size (basal width, volume), summit size (W_S/W_B) and complexity (increase in *ei*, *ii*, and peak count), and of decreasing steepness (decrease in H/W_B and slope values; Fig. 5). This transition is similar to the morphometric evolution of arc volcanoes from ‘cones’ to ‘sub-cones’ to ‘massifs’ proposed by Grosse et al. (2009). However, overlap and spread are very large. In particular, the ‘stratovolcano’ group spans two-thirds of entries and contains edifices with very

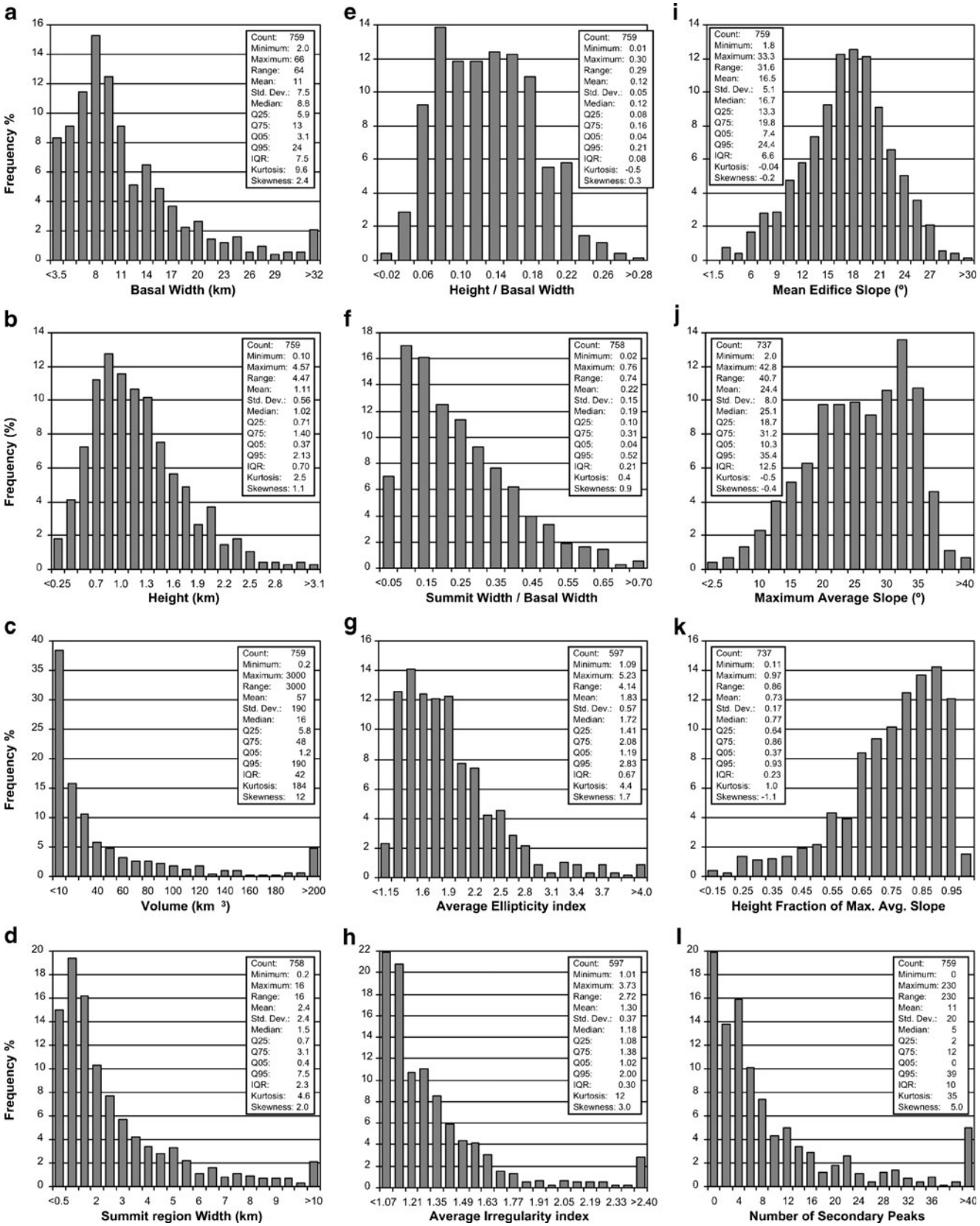

Fig. 3 **a**–**l** Frequency histograms and statistics of main morphometric parameters. Bin size determined using the Freedman-Diaconis rule. For the average ellipticity and irregularity index values, only edifices with five or more closed elevation contours on flanks are considered ($n = 597$). Values in the X-axes are the upper bin limits

variable morphologies. Also, the 'stratovolcanoes' and 'complex/compound volcano' groups have very similar average values for most parameters. A more rigorous classification based on quantitative data is thus desirable; the database here presented could be used to this end.

Curves of ellipticity index, irregularity index, and slopes vs. height

The *ei* and *ii* values of successive elevation contours define two independent curves that together summarize edifice plan shape. Similarly, the average slope of successive height intervals can be considered a profile shape 'fingerprint' (Grosse et al. 2012). The values and shapes of these fingerprints can vary greatly; see Grosse et al. (2012) for a case study of Nicaraguan volcanoes. Figure 6 shows average curves considering volcanoes with at least five closed flank contours (for the *ei* and *ii* profiles, 597 entries) and ten slope bins (for the slope profile, 704 entries). Figure 7 shows schematic diagrams that summarize the frequency of curve shapes considering four height intervals and three possible paths at each interval: decrease, equal, and increase.

Although almost all possible curve shapes are found, some generalizations can be made:

- Ellipticity tends to increase with height, especially in the upper half of flanks. In 70 % of edifices the uppermost height interval is more elliptical than the lowermost interval. A preferential elongation towards the summit region can be related to vent migration, collapse-generated arcuate ridges, and prevailing winds that channel tephra fallout.
- Irregularity index curves are the most variable of the three. In the lower half of flanks the index tends to decrease or keep steady, whereas in the upper half no clear tendency is found. Overall, the index more commonly decreases towards the summit. This can be related to a greater development of valleys or gullies down-slope, the presence of secondary vents on lower flanks, possible interaction with the pre-volcano surface and gravitational deformation.
- Slopes tend to increase with height up to around 80–90 % of the edifice height and then strongly decrease in the uppermost summit region. Maximum slopes can also occur at lower height fractions, this is especially common at shield volcanoes. Topographic complexities at the lower flanks tend to produce more scattered values and profile segments. Slope increase is most evident in the middle-height intervals, approximately coincident with the main flanks. Sixty to 70 % of edifices show slope increase in these height intervals, and in over 90 % of edifices the uppermost flanks are steeper than the lower flanks. The upper height interval has more erratic slope profiles as it includes the summit region, where complexities of vents, domes, and crater dynamics would have an influence. The overall increase of slopes with height can be related with the evolution of edifices towards steady-state or equilibrium concave-up profiles controlled by gravity-driven mass transfer (e.g., Davidson and De Silva 2000).

Fig. 4 Selected X–Y plots of morphometric parameters. Data are grouped by morphological type and by underwater extent (whether they continue underwater or not); symbol reference in (**k**). In **g** to **k**, average ellipticity and irregularity index values are of edifices with five or more closed elevation contours on flanks (n = 597)

Examples

The wide range of existing volcano morphometries is illustrated in Fig. 8 through seven examples:

- Mayon (Luzon, Philippines) is an end-member example of a symmetrical and steep cone (the 'textbook' stratovolcano); it has a high H/W_B ratio and very low W_S/W_B ratio and *ei* and *ii* values, indicating a circular and smooth plan shape, although *ii* increases slightly towards the base due to a gully on the NW flank; slopes smoothly increase with height, reaching values >35° before dropping in the small summit region.
- Aracar (Central Andes, Argentina) is a steep and quite smooth cone with some minor complexities; its H/W_B ratio and slopes are above average, whereas its W_S/W_B ratio and *ei* and *ii* values are below average; the *ii* is low and constant, whereas the *ei* has a strong mid-flank increase caused by a SE-trending ridge (with a secondary peak); it has a summit crater that is considered the summit region.
- Sakura-jima (Kyushu, Japan) has morphometric values of size, shape, and slope that are close to the average values of the whole database; the *ei* increases with height due to the presence of several summit region vents.
- Kelut (Java, Indonesia) is an example of a very irregular edifice with high *ii* values caused by strong dissection; the W_S/W_B ratio is close to average, whereas the H/W_B ratio is below average; slopes and *ei* increase towards the summit.
- Rincón de la Vieja (Costa Rica) is an example of an elongated massif with several peaks in the summit region; it has a low H/W_B ratio and a high W_S/W_B ratio; the *ei* is high and strongly increases towards the summit region; slopes are relatively low and increase with height.
- Nemrut Dagi (Turkey) is an example of an edifice truncated by a very large crater (which is considered the summit region); it thus has a high W_S/W_B ratio and a low H/W_B ratio; slopes are low and show an irregular trend with height; there are no closed elevation contours between the edifice and the crater outlines, so there are no *ei* and *ii* values.

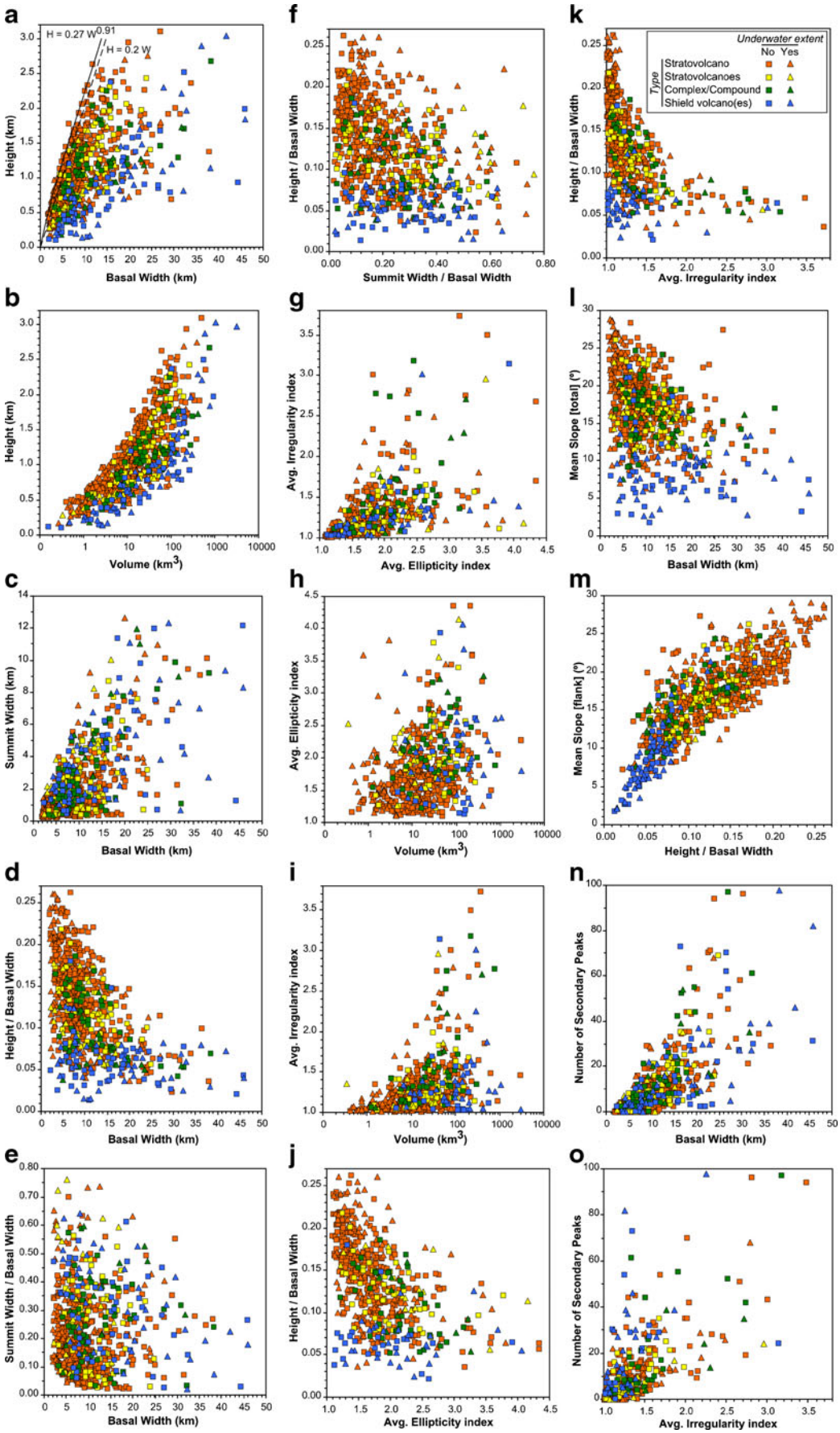
a
H = 0.27 W^0.91
H = 0.2 W
Height (km)
Basal Width (km)
f
Height / Basal Width
Summit Width / Basal Width
k
Underwater extent
No Yes
Type
Stratovolcano
Stratovolcanoes
Complex/Compound
Shield volcano(es)
Height / Basal Width
Avg. Irregularity index
b
Height (km)
Volume (km3)
g
Avg. Irregularity index
Avg. Ellipticity index
l
Mean Slope [total] (°)
Basal Width (km)
c
Summit Width (km)
Basal Width (km)
h
Avg. Ellipticity index
Volume (km3)
m
Mean Slope [flank] (°)
Height / Basal Width
d
Height / Basal Width
Basal Width (km)
i
Avg. Irregularity index
Volume (km3)
n
Number of Secondary Peaks
Basal Width (km)
e
Summit Width / Basal Width
Basal Width (km)
j
Height / Basal Width
Avg. Ellipticity index
o
Number of Secondary Peaks
Avg. Irregularity index

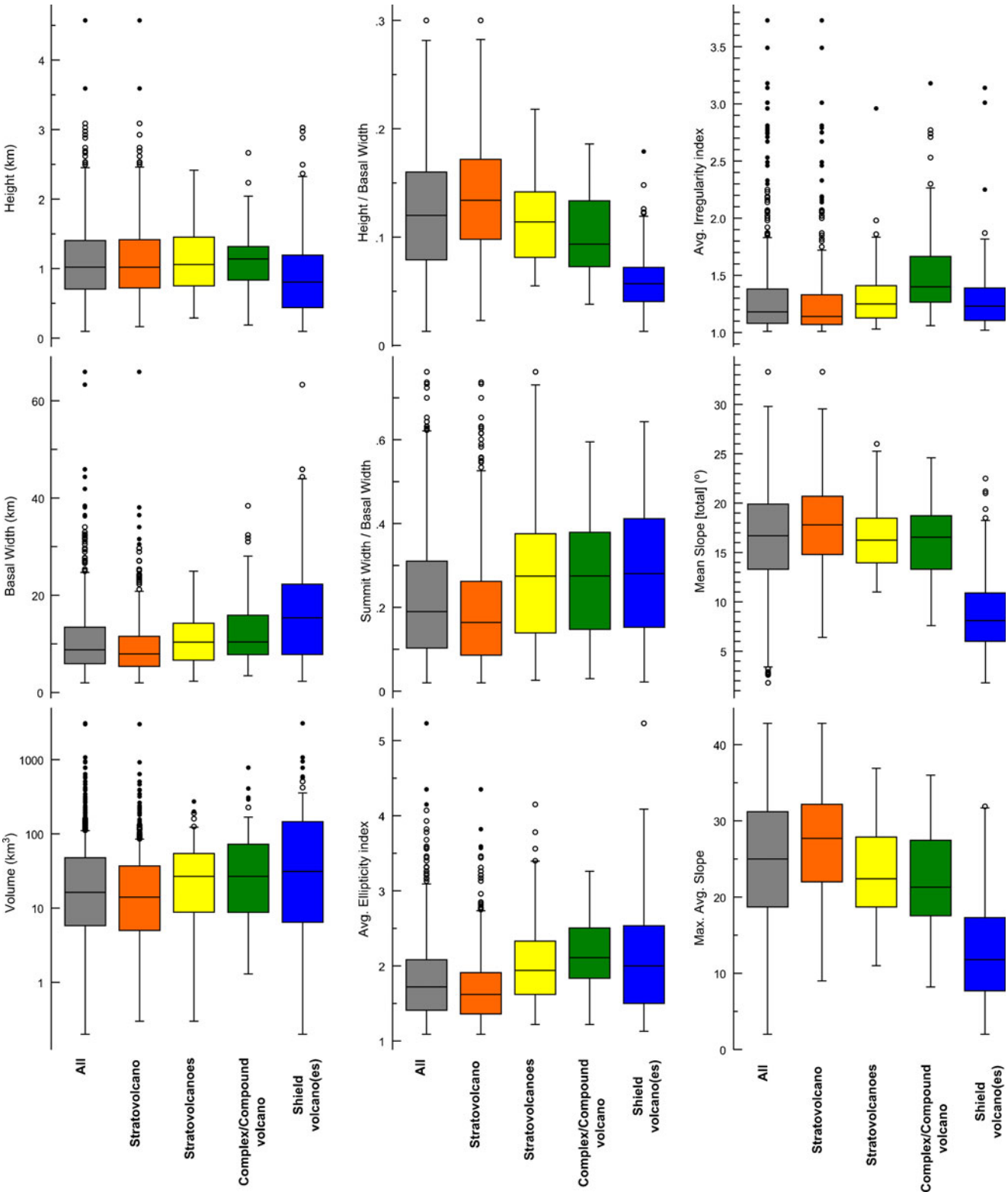

Fig. 5 Box-and-whisker plots summarizing the statistical properties of the main morphometric parameters for all entries and according to four main morphological types following the Smithsonian Institution Global Volcanism Program database. *Bottom and top of boxes* are the lower and upper quartiles, respectively; *inner line* is the median; *whiskers* span values within 1.5 times the inter-quartile range; *outside open circles* are values >1.5×IQR; *far outside filled circles* are values >3×IQR

– Aoba (SW Pacific, Vanuatu) is a large shield with low slopes and a low H/W_B ratio; it has a summit crater within a relatively flat summit region; the slope curve has a smooth hump-back shape with maximum values relatively low on

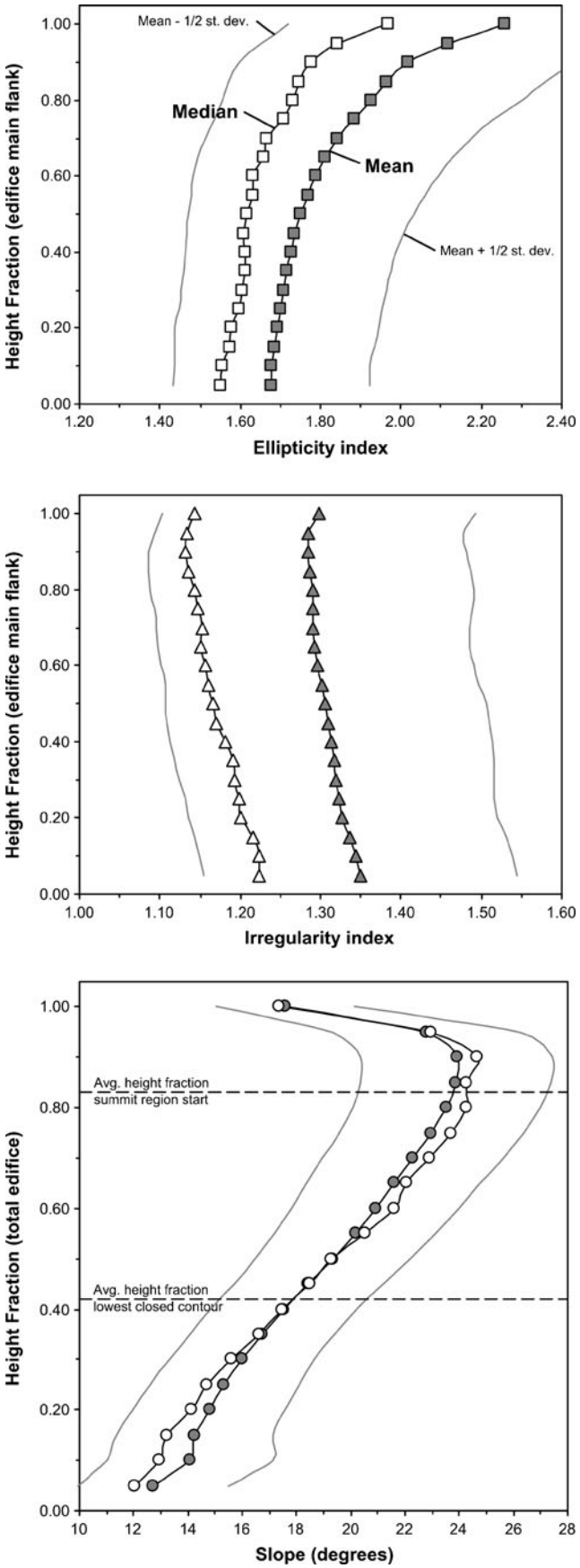

◀ **Fig. 6** Mean and median average profiles of ellipticity index (*ei*), irregularity index (*ii*), and slope vs. height considering edifices with at least five closed flank contours for the *ei* and *ii* profiles ($n = 597$), and with at least ten slope bins for the slope profile ($n = 704$)

the flank; the *ei* has an unusual decreasing trend from very high elongation at the base to a very circular summit region; the *ii* slightly decreases with height.

Database access and future development

In addition to the present contribution, we are working on the development of a website for online access of the database. The edifice and crater outlines will be uploaded, as well as plan and profile images and graphs for each volcano. We also plan to make available user-friendly versions of the NETVOLC and MORVOLC algorithms.

Through the website, future developments and updates will be made available. Planned future work includes: addition of volcanoes to the database, eventually extending it to incorporate Pleistocene volcanoes listed in the GVP; supplementary databases of volcanoes not covered by the SRTM DEM using other DEMs; addition of underwater data using bathymetric DEMs; generation of new databases using higher-resolution DEMs (e.g., the soon to be released global TanDEM-X dataset); extension of the summit crater dataset using higher-resolution DEMs; and NETVOLC and MORVOLC updates, including the development of new morphometric parameters and of an algorithm for automatic delineation of summit craters. The website will also enable feedback from the scientific community, including report of errors and bugs.

Conclusions

The presented database is a systematic and comparable near-global database on the subaerial morphometry of composite volcanoes with basal widths greater than 2 km. The use of: (1) a single and continuous data source, the seamless SRTM DEM, (2) a single semi-automatic method, NETVOLC, for delimitation of volcano edifice boundaries, and (3) a single code for computation of parameters, MORVOLC, maximizes consistency, accuracy, and comparability throughout the database.

The database contains 759 entries of Holocene, active and potentially active, composite volcanoes from around the World. The parameters thoroughly characterize the morphometry of each volcano edifice in terms of size, profile shape, plan shape, and slopes. Main drawbacks

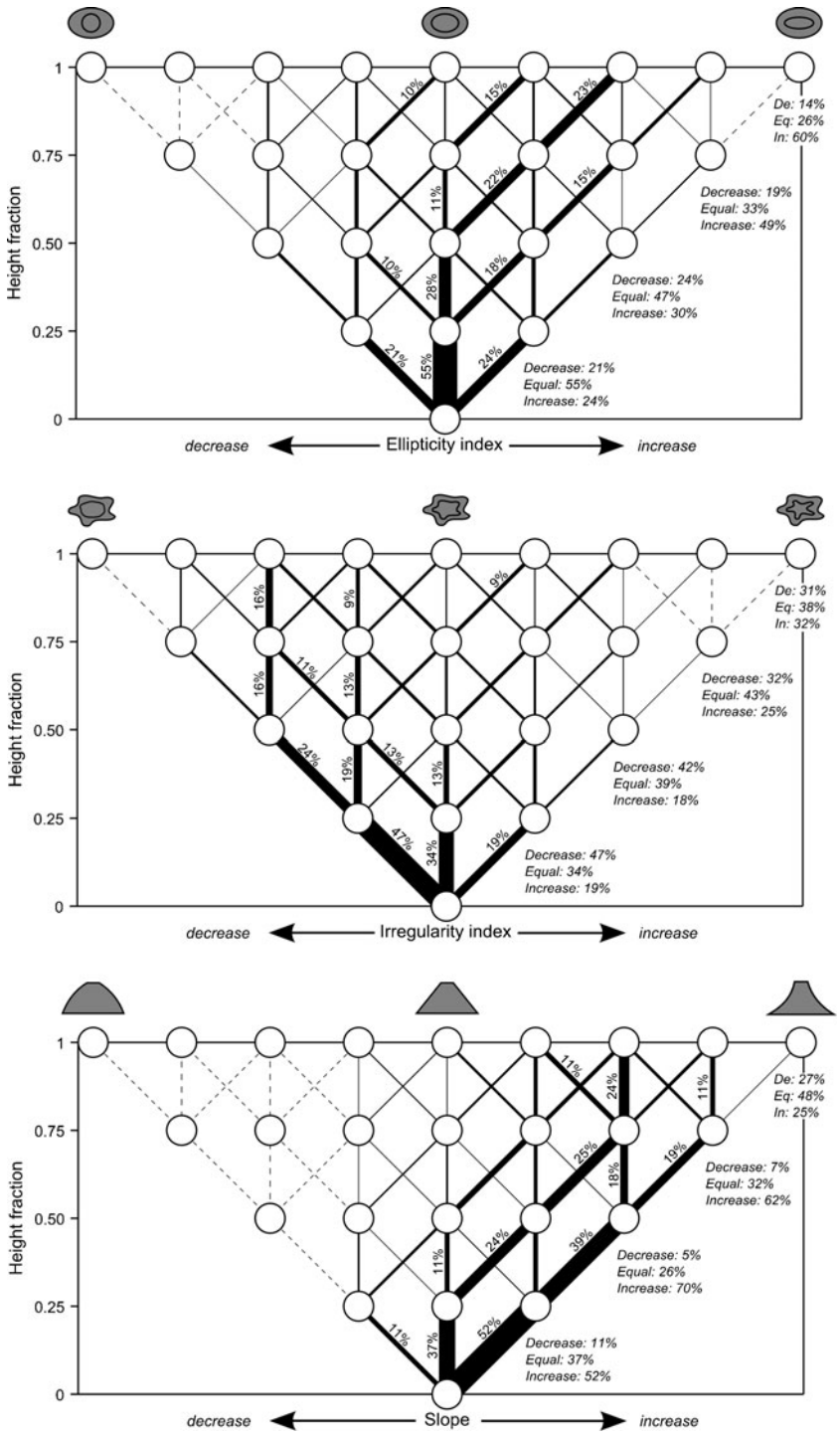

Fig. 7 Schematic frequency diagrams of the shapes produced by the ellipticity index, irregularity index, and slope vs. height profiles, considering four height intervals and three possible paths at each interval: decrease, equal, and increase. Thicknesses of profile segments are proportional to frequency; *dashed lines* indicate segments with <1 % frequency. For each height interval, the percent frequencies of the three most frequent segments are given, and the overall frequency of path decrease, equality, and increase are shown to the right of the diagram. For the ellipticity and irregularity diagrams, edifices with ten or more closed flank contours were considered (n =396); for the slope diagram, edifices with 20 or more slope bins were considered (n =553)

are the exclusion of small edifices (basal widths<2 km), the incompleteness of the summit crater dataset, and the lack of underwater data. These limitations are inherent of the data source resolution and coverage; higher-resolution and bathymetric DEMs are needed to resolve these issues.

Most parameters show large variation suggesting a whole continuum of morphologies lacking clear separations (as previously pointed out by Pike 1978). Analysis of the main GVP morphologic types indicates that the existing classification does not match the existing morphometric variability. The continuum in parameter values reflects the fact that volcano morphology is the result of a combination of several constructional, erosional, and structural processes that can vary between volcanoes

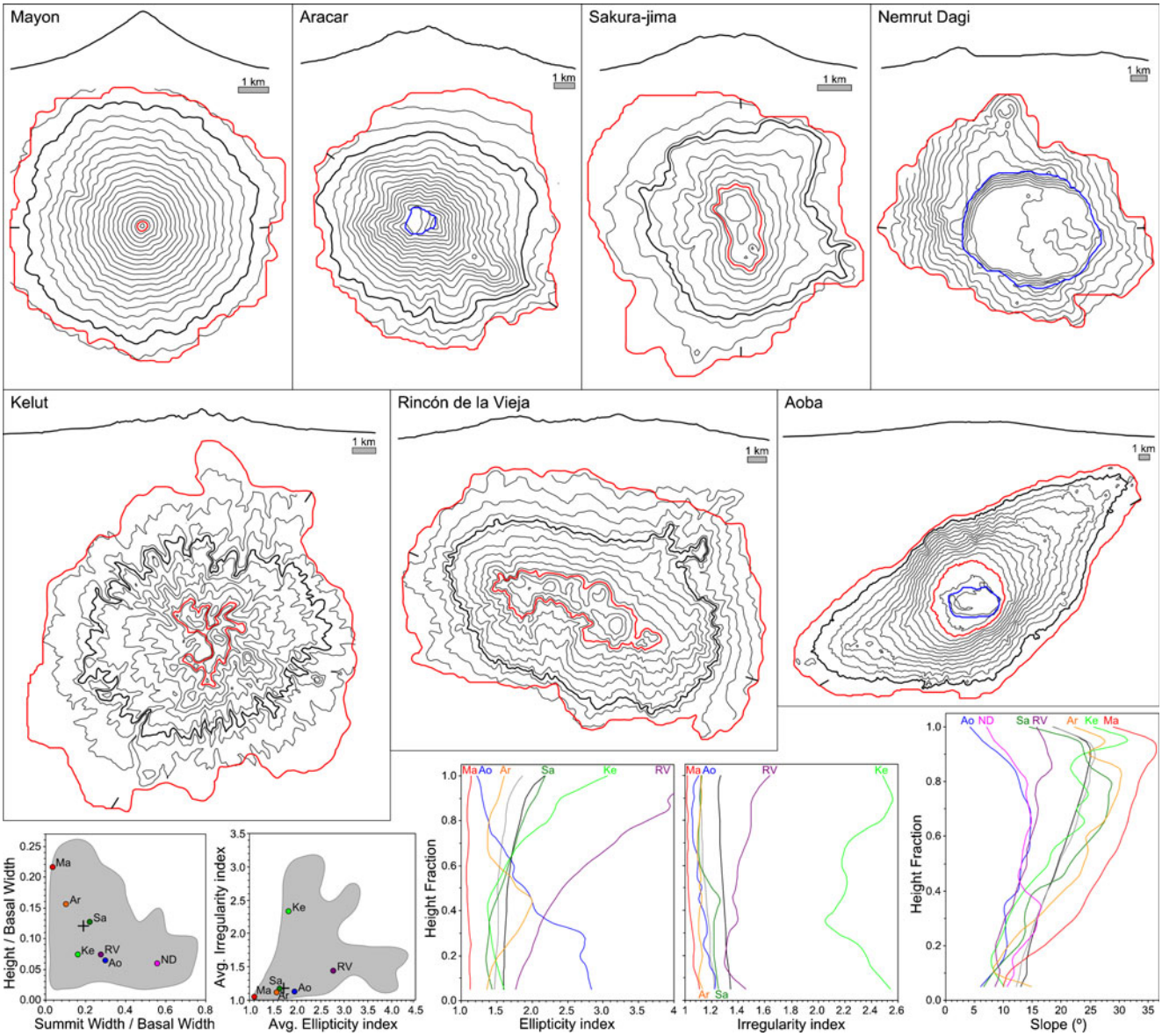

Fig. 8 Examples of different volcano edifice morphometries. For each volcano, a profile (no vertical exaggeration) and a plan view are shown; elevation contours (every 100 m) are in *black*, *thicker black contour* is the lowest closed contour; edifice and summit region outlines are in *red*; summit crater outlines are in *blue*; *black tick marks* indicate location of profiles. *Bottom left* height/basal width vs. summit width/basal width and average irregularity vs. average ellipticity diagrams with the examples plotted; *gray fields* are the distribution of all database entries (excluding outliers); and *black crosses* are the median values of the whole database. *Bottom right* ellipticity, irregularity, and slope vs. height curves of the examples; *black and gray curves* are the mean and median averages, respectively, of the whole database (see Fig. 6). *Ma* Mayon, *Ar* Aracar, *Sa* Sakura-jima, *ND* Nemrut Dagi, *Ke* Kelut, *RV* Rincón de la Vieja, *Ao* Aoba

and within a single edifice with time. Nevertheless, detailed statistical analyses (such as clustering, e.g., Hone et al. 2007) of the morphometric parameters can potentially lead to the identification of processes and pave the way for a more rigorous quantitative classification of volcano morphology that is linked to the controlling factors.

We expect that the database will be useful as a research tool for volcanological studies at different scales including global, regional, local, and individual. It can be used for comparative studies and for quantitative and systematic classifications, and should also allow systematic planetary comparisons. The database will be maintained and updated through a website under preparation.

Acknowledgments PG is grateful to CONICET and Fundación Miguel Lillo for their support. We thank R. J. Pike and an anonymous reviewer, as well as Editor A. Gudmundsson, for their reviews and comments. We are also grateful to M. Kervyn for his informal comments and suggestions.

References

Carr MJ (1984) Symmetrical and segmented variation of physical and geochemical characteristics of the Central American Volcanic Front. J Volcanol Geotherm Res 20:231–252

Carr MJ, Saginor I, Alvarado GE, Bolge LL, Lindsay FN, Milidakis K, Turrin BD, Feigeson MD, Swisher CC (2007) Element fluxes from the volcanic front of Nicaragua and Costa Rica. Geochem Geophys Geosyst 8:Q06001

Committee for catalog of Quaternary Volcanoes in Japan (Eds.) (1999) Catalog of Quaternary volcanoes in Japan. The Volcanological Society of Japan

Davidson J, De Silva S (2000) Composite volcanoes. In: Sigurdsson H et al. (eds) Encyclopedia of Volcanoes. Academic Press, pp. 663–681

De Silva SL, Francis PW (1991) Volcanoes of the Central Andes. Springer, New York, p 216

Euillades LD, Grosse P, Euillades PA (2013) NETVOLC: an algorithm for automatic delimitation of volcano edifice boundaries using DEMs. Comput Geosci 56:151–160

Evans IS (2012) Geomorphometry and landform mapping: what is a landform? Geomorphology 137:94–106

Favalli M, Karátson D, Mazzuoli R, Pareschi MT, Ventura G (2005) Volcanic geomorphology and tectonics of the Aeolian archipelago (Southern Italy) based on integrated DEM data. Bull Volcanol 68: 157–170

Favalli M, Karátson D, Mazzarini F, Pareschi MT, Boschi E (2009) Morphometry of scoria cones located on a volcano flank: a case study from Mt. Etna (Italy), based on high-resolution LiDAR data. J Volcanol Geotherm Res 186:320–330

Fedotov SA, Masurenkov YP (1991) Active volcanoes of Kamchatka, vol 1. Nauka, Moscow, p 302, Vol. 2, pp. 415

Fornaciai A, Favalli M, Karátson D, Tarquini S, Boschi E (2012) Morphometry of scoria cones, and their relation to geodynamic setting: a DEM-based analysis. J Volcanol Geotherm Res 217–218:56–72

Grosse P, van Wyk de Vries B, Petrinovic IA, Euillades PA, Alvarado G (2009) Morphometry and evolution of arc volcanoes. Geology 37: 651–654

Grosse P, van Wyk de Vries B, Euillades PA, Kervyn M, Petrinovic IA (2012) Systematic morphometric characterization of volcanic edifices using digital elevation models. Geomorphology 136:114–131

Hone DWE, Mahony SH, Sparks RSJ, Martin KT (2007) Cladistic analysis applied to the classification of volcanoes. Bull Volcanol 70:203–220

Jarvis A, Reuter HI, Nelson A, Guevara E (2008) Hole-filled SRTM for the globe Version 4: CGIAR-CSI SRTM 90 m Database (http://srtm.csi.cgiar.org)

Karátson D, Favalli M, Tarquini S, Fornaciai A, Wörner G (2010) The regular shape of stratovolcanoes: a DEM-based morphometrical approach. J Volcanol Geotherm Res 193:171–181

Karátson D, Telbisz T, Wörner G (2012) Erosion rates and erosion patterns of Neogene to Quaternary stratovolcanoes in the Western Cordillera of the Central Andes: an SRTM DEM based analysis. Geomorphology 139–140:122–135

Kervyn M, Ernst GGJ, Goossens R, Jacobs P (2008) Mapping volcano topography with remote sensing: ASTER vs. SRTM. Int J Remote Sens 29:6515–6538

Kervyn M, Ernst GGJ, Carracedo J-C, Jacobs P (2012) Geomorphometric variability of "monogenetic" volcanic cones: evidence from Mauna Kea, Lanzarote and experimental cones. Geomorphology 136:59–75

Kozhemyaka NN (1995) Active volcanoes of Kamchatka: types and growth times of cones, total volumes of erupted material, productivity, and composition of rocks. Volcanol Seismol 16:581–594

Mathieu L, van Wyk de Vries B, Mannessiez C, Mazzoni N, Savry C, Troll VR (2013) The structure and morphology of the Basse Terre Island, Lesser Antilles volcanic arc. Bull Volcanol 75:700

Miller TP, McGimsey RG, Richter DH, Riehle JR, Nye CJ, Yount ME, Dumoulin JA (1998) Catalog of the historically active volcanoes of Alaska. U.S. Geological Survey Open-File Report 98–582

Mitchell NC, Stretch R, Oppenheimer C, Kay D, Beier C (2012) Cone morphologies associated with shallow marine eruptions: east Pico Island, Azores. Bull Volcanol 74:2289–2301

Mouginis-Mark PJ, Rowland SK, Garbeil H (1996) Slopes of western Galapagos volcanoes from airborne interferometric radar. Geophys Res Lett 23:3767–3770

Pike RJ (1978) Volcanoes on the inner planets: some preliminary comparisons of gross topography. 9th Lunar and Planetary Science Conference, pp. 3239–3273

Pike RJ, Clow GD (1981) Revised classification of terrestrial volcanoes and a catalog of topographic dimensions with new results on edifice volume, U.S. Geological Survey Open-File Report OF 81–1038

Plescia JB (2004) Morphometric properties of Martian volcanoes. J Geophys Res 109, E03003

Rabus B, Eineder M, Roth A, Bamler R (2003) The shuttle radar topography mission—a new class of digital elevation models acquired by spaceborne radar. ISPRS J Photogramm Remote Sens 57:241–262

Reuter HI, Nelson A, Strobl P, Mehl W, Jarvis A (2009) A first assessment of ASTER GDEM tiles for absolute accuracy, relative accuracy and terrain parameters. Proc 2009 I.E. Int Geosci Remote Sens Symp (IGARSS) 5:240–243

Rodríguez E, Morris CS, Belz JE (2006) A global assessment of the SRTM performance. Photogramm Eng Remote Sens 72: 249–260

Rowland SK, Garbeil H (2000) Slopes of oceanic volcanoes. In: Mouginis-Mark P, Crisp J, Fink J (eds) Remote sensing of active volcanism. Geophysical Monograph, American Geophysical Union, pp. 223–247

Settle M (1979) The structure and emplacement of cinder cone fields. Am J Sci 279:1089–1107

Siebert L, Simkin T, Kimberly P (2010) Volcanoes of the World, 3rd edition. University of California Press, pp. 551

Smith MJ, Clark CD (2005) Methods for the visualization of digital elevation models for landform mapping. Earth Surf Proc Land 30: 885–900

Stoiber RE, Carr MJ (1973) Quaternary volcanic and tectonic segmentation of Central America. Bull Volcanol 37:304–325

Stretch RC, Mitchell NC, Portaro RA (2006) A morphometric analysis of the submarine volcanic ridge south-east of Pico Island, Azores. J Volcanol Geotherm Res 156:35–54

van Wyk de Vries B, Grosse P, Alvarado GE (2007) Volcanism and volcanic landforms. In: Bundschuh J, Alvarado GE (eds) Central America: geology, resources and hazards. Balkema, Rotterdam, pp 123–158

Völker D, Kutterolf S, Wehrmann H (2011) Comparative mass balance of volcanic edifices at the southern volcanic zone of the Andes between 33°S and 46°S. J Volcanol Geotherm Res 205:114–129

Wood CA, Kienle J (1990) Volcanoes of North America: United States and Canada. Cambridge University Press, pp. 354

Wright R, Garbeil H, Baloga SM, Mouginis-Mark PJ (2006) An assessment of shuttle radar topography mission digital elevation data for studies of volcano morphology. Remote Sens Environ 105:41–53